# Characterization of Pt@Cu Core@Shell Dendrimer-Encapsulated Nanoparticles Synthesized by Cu Underpotential Deposition

Emily V. Carino and Richard M. Crooks*

Department of Chemistry and Biochemistry, Center for Electrochemistry, and the Texas Materials Institute, The University of Texas at Austin, 1 University Station, A5300, Austin, Texas 78712-0165, United States

Ⓢ *Supporting Information*

ABSTRACT: Dendrimer-encapsulated nanoparticles (DENs) containing averages of 55, 147, and 225 Pt atoms immobilized on glassy carbon electrodes served as the electroactive surface for the underpotential deposition (UPD) of a Cu monolayer. This results in formation of core@shell (Pt@Cu) DENs. Evidence for this conclusion comes from cyclic voltammetry, which shows that the Pt core DENs catalyze the hydrogen evolution reaction before Cu UPD, but that after Cu UPD this reaction is inhibited. Results obtained by in situ electrochemical X-ray absorption spectroscopy (XAS) confirm this finding.
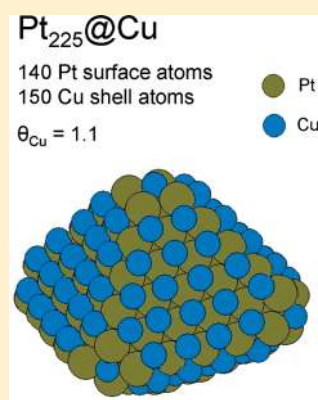
■ INTRODUCTION

Here we report the electrochemical synthesis of Pt core/Cu shell (Pt$_n$@Cu, $n = \sim$55, 147, and 225 Pt atoms) dendrimer-encapsulated nanoparticles (DENs).[1] These materials are prepared as shown in Scheme 1. First, Pt DENs are synthesized by encapsulating Pt^{2+} within sixth-generation, hydroxyl-terminated poly(amidoamine) (PAMAM) dendrimers (G6-OH) to yield a metal/dendrimer complex (G6-OH(Pt^{2+})$_n$). Second, the complexes are reduced with BH$_4^-$. Third, the resulting Pt DENs (G6-OH(Pt$_n$)) are purified and immobilized on a glassy carbon (GC) or carbon paper electrode. Finally, a monolayer of Cu is electrodeposited onto the Pt DENs by underpotential deposition (UPD) to yield G6-OH(Pt$_n$@Cu) DENs. Results obtained from voltammetry and in situ X-ray absorption spectroscopy (XAS) confirm the core@shell structural configuration. The findings reported here are significant for four reasons. First, this method for synthesizing bimetallic DENs greatly expands the variety of shell metals that can be incorporated into core@shell DENs. Second, we demonstrate that this method is applicable to nanoparticles having cores containing as few as ~55 atoms. Third, UPD is a monolayer-specific and potential-dependent process, and therefore, the resulting DENs have well-defined structures. Fourth, the UPD process can be used to selectively decorate particular crystallographic faces,[2−4] and therefore, there is an opportunity in the future to study the catalytic properties of bimetallic DENs having just partial shell coverage.

Near-surface alloys (NSAs), which are two-dimensional analogues of core@shell nanoparticles, have interesting and often unanticipated catalytic properties.[5−8] Accordingly, we have been interested in developing methods for synthesizing catalytically active core@shell DENs containing just a few hundred atoms. Like NSAs, DENs in the 1−2 nm size range are compatible with first-principles calculations,[9] and thus, they provide a means for direct comparison of experimental and theoretical studies of the effect of catalyst structure on reaction rates and selectivity.

We have previously shown that core@shell DENs can be synthesized by the sequential reduction of the component metals.[10,11] However, there are some limitations to this method. First, the size monodispersity of DENs synthesized by sequential reduction is generally not as good as that of the monometallic cores.[10,11] Second, because the reducing power of chemical reductants is quantized, it is difficult or impossible to strictly control the number of shell atoms deposited on the core. Third, it is impossible to selectively control deposition of the shell metal on particular crystallographic locations of the core. In contrast, electrochemical methods provide fine energy resolution and thus a much higher level of control over the shell structure.[12−21] For example, Adzic and co-workers synthesized Pt-shell nanoparticles by UPD of Cu onto Pd nanoparticles, followed by galvanic exchange of Cu for Pt.[21] The average diameter of the resulting Pd@Pt nanoparticles was 4.2 nm. XAS confirmed the core@shell structure and the presence of a single monolayer of Pt. A similar approach was used to synthesize Pt monolayer shells on nanoparticle cores of Au[3,14] and Ru.[3]

Scheme 1
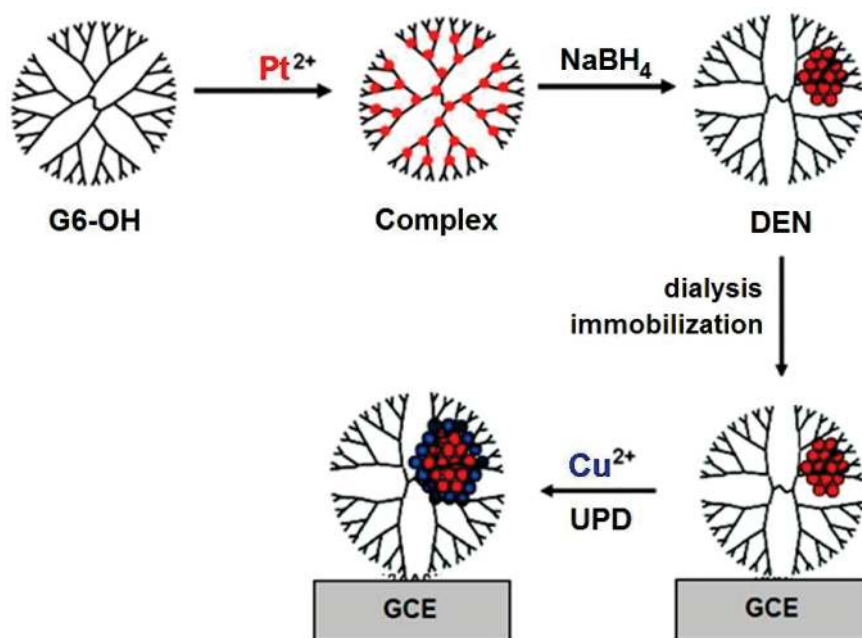
More recently, this method has been applied to the formation of Pt—M mixed monolayers on Pd cores, where M = Au, Pd, Rh, Ir, Os, or Re.[21] UPD, which allows for the controlled, surface-selective deposition of a metal monolayer, is an essential step in the synthesis of these well-defined nanostructures.

We recently presented preliminary results for the synthesis of core@shell Au@Pt DENs synthesized via Cu UPD onto Au DENs, followed by galvanic exchange of the Cu shell for Pt.[22] Preliminary measurements of the electrocatalytic activity of these materials for the oxygen reduction reaction were also described.[22] In this more comprehensive study, three sizes of Pt DENs were prepared and used as substrates for Cu UPD. The results indicate that a single atomic monolayer of Cu is deposited onto Pt DEN cores containing averages of 147 and 225 atoms, while more than one monolayer deposits onto Pt DEN cores containing an average of 55 atoms. Structural analysis of G6-OH(Pt_{225}@Cu) DENs by in situ XAS reveals a Pt-rich core and Pt—Cu and Cu—Cu bonding that is consistent with the proposed core@shell structure.

■ EXPERIMENTAL SECTION

Chemicals. G6-OH dendrimers were purchased from Dendritech, Inc. (Midland, MI) as 10.0 wt % solutions in methanol. Prior to use, the methanol was removed under vacuum and the dendrimers were redissolved in sufficient water to yield a 0.10 mM solution. Unless otherwise noted, HPLC-grade water (Fisher Scientific) was used to prepare all aqueous solutions. K_2PtCl_4, $CuSO_4$, $LiClO_4$, $NaBH_4$, and Ultrex ultrapure H_2SO_4 (18.76 M) were purchased from Sigma-Aldrich (Milwaukee, WI). These reagents were used as received without further purification.

Synthesis of Pt DEN Cores. Pt DENs were prepared according to our previously published procedure.[23] Briefly, a 0.10 mM aqueous solution of G6-OH was mixed with sufficient aqueous 0.10 M K_2PtCl_4 such that the final Pt^{2+}-to-dendrimer ratios were 55:1, 147:1, or 225:1. The solutions were stirred for 3 days to ensure complete complexation of Pt^{2+} with the interior tertiary amines of the dendrimers.[24] The

Pt^{2+}/G6-OH complexes resulting from this first synthetic step are denoted as G6-OH$(Pt^{2+})_n$ (n = 55, 147, and 225). The second step of the synthesis involves reduction of G6-OH$(Pt^{2+})_n$ with a 10-fold molar excess of 1.0 M $NaBH_4$. Immediately following addition of $NaBH_4$, the reaction vessel was tightly sealed so that H_2 gas, generated by the reaction between BH_4^- and water, was retained. This solution was stirred for 24.0 h to ensure complete reduction of Pt^{2+}.[24] Following the reduction step, but before use in electrochemical experiments, the DENs were dialyzed for 24.0 h in 4.0 L of Millipore water (Milli-Q Gradient PF-06073) to remove salts and other impurities. The water was exchanged midway through the dialysis. After dialysis, but prior to immobilization onto GC electrodes, the DEN solution was mixed with an appropriate volume of aqueous 1.0 M $LiClO_4$ to yield solutions having final $LiClO_4$ concentrations of 0.10 M.

Electrochemistry. Both the Au-wire counter electrode and the fritted Hg/Hg_2SO_4 reference electrode were purchased from CH Instruments (Austin, TX) and used for all electrochemical experiments unless otherwise specified. All potentials are reported vs NHE. Several different types of working electrodes were used in this study, including (1) a 3 mm diameter, GC disk electrode (CH Instruments, Austin, TX); (2) AvCarb p75 carbon fiber paper (Ballard Materials Products); and (3) a 2 mm diameter polycrystalline Pt disk electrode (CH Instruments, Austin, TX).

The GC disk electrode was prepared by successive mechanical polishing with 1.0, 0.3, and 0.05 μm alumina, ultrasonicating in a 50:50 water—ethanol mixture for 1 min, and finally electrochemical anodizing in 0.10 M NaOH.[25] The latter process was carried out by stepping the electrode potential from its open circuit value to 1.20 V (vs NHE) and then holding it at this potential for 30 s. The polishing procedure for the Pt disk electrode was the same as for the GC electrodes. The AvCarb paper electrodes were rendered hydrophilic by cycling their potentials eight times between 1.64 and −0.37 V in 0.50 M H_2SO_4.[26]

Pt DENs were immobilized on GC working electrodes by cycling the potential three times between 0.24 and 1.24 V in a solution containing the DENs and 0.10 M $LiClO_4$.[23] After Pt DEN immobilization, but before UPD, the DENs were electrochemically cleaned by cycling them 10 times between −0.03 and 1.34 V in a deoxygenated, aqueous 0.10 M

H_2SO_4 solution.[27] Deoxygenation was accomplished by purging the solution with Ar for 10 min prior to potential cycling. During these scans, waves corresponding to the adsorption and desorption of hydrogen became increasingly more prominent and eventually attained a steady-state shape and magnitude, signaling a clean Pt surface (Supporting Information, Figure S1).[27] Immediately after this cleaning procedure, a background cyclic voltammogram (CV) of the Pt DENs was obtained in Cu-free electrolyte solution.

Cu UPD onto the Pt DENs was carried out using the following procedure. First, the electrode potential was stepped from the open-circuit potential (OCP) to 0.64 V for 150 s as a pretreatment. Similar methods have been used to obtain maximum Cu monolayer coverage on Pt electrodes.[28,29] Second, the potential was swept from 0.64 to 0.84 V, negative to 0.28 V, and then back to 0.84 V. Finally, the DEN-modified electrode was transferred back to the Cu-free solution and a final CV was collected for comparison to the one obtained before exposure to Cu.

Electrodes for XAS analysis were prepared by soaking the electro-chemically oxidized carbon paper in a solution of dialyzed 10.0 μM G6-OH(Pt_{225}) for 24.0 h and then rinsing with water. The immobilized Pt DENs were electrochemically cleaned in 0.10 M H_2SO_4 prior to XAS experiments using the same procedure described for the DEN-modified GC electrodes. Next, a potential step from the OCP to -0.10 V was applied for 15 min to ensure complete reduction of the DENs prior to XAS analysis.[26] The cell was then filled with a solution containing 0.10 M H_2SO_4 and 0.010 M $CuSO_4$, and preliminary XAS scans of bare G6-OH(Pt_{225}) were collected at OCP prior to depositing Cu. The solutions were not deoxygenated due to constraints imposed by the design of the in situ cell. Care was taken while filling the cell so that it did not contain any air pockets, and the cell remained sealed during the experiments.

Before collecting in situ XAS spectra, a CV was obtained to determine the potential at which one monolayer of Cu is deposited by UPD (E_{UPD}) (Supporting Information, Figure S2). E_{UPD} was found to be 0.26 V vs NHE in the in situ XAS cell. In situ XAS data were obtained at two potentials: E_{UPD} and E_{bare}, where $E_{bare} = 0.84$ V, a potential where no Cu is deposited. The working electrode potential was stepped from the OCP to E_{bare} and held there while XAS data were acquired. Without returning to OCP, the potential was stepped from E_{bare} to E_{UPD} to deposit one monolayer of Cu. After the current due to Cu UPD decreased to a steady-state value close to 0, indicating the completion of the UPD process, the cell was turned off while the Cu^{2+}-containing solution was removed and the cell refilled with Cu^{2+}-free 0.10 M H_2SO_4. The solution exchange process took less than 90 s, after which the cell was reconnected at E_{UPD}. It was prudent to exchange the Cu^{2+}-containing solution for Cu^{2+}-free 0.10 M H_2SO_4 prior to collecting XAS spectra of the Cu-edge, because the X-ray absorbance due to the free Cu^{2+} in solution would mask the absorbance due to Cu atoms on the surface of the DENs. Experiments carried out after the solution exchange confirmed that the full Cu monolayer was retained and the absence of free Cu^{2+} in the solution (Supporting Information, Figures S3 and S4). XAS spectra of G6-OH(Pt_{225}@Cu) were collected once the current at E_{UPD} attained a steady-state value close to 0. The cell potential was held at E_{UPD} during XAS data acquisition. Finally, the Cu shell was stripped by sweeping the potential from E_{UPD} to E_{bare} (Supporting Information, Figure S3) and additional XAS spectra were collected.

Electrochemical measurements obtained using the GC electrode were made in glass scintillation vials that were triply rinsed with Millipore water prior to use. The experiments using carbon paper electrodes were performed in a Teflon cell that was specifically designed for in situ XAS experiments (Supporting Information, Figure S5). CVs using GC electrodes were obtained using a CHI 760B potentiostat (CH Instruments). The in situ XAS experiments were carried out using a WaveNow hand-held potentiostat (Pine Instruments, Grove City, PA).

Characterization. UV−vis absorption spectra were collected using a Hewlett-Packard HP8453 UV−vis spectrometer and a quartz cuvette

having an optical path length of 0.100 cm (Starna Cells, Inc., Atascadero, CA). The DENs spectra were referenced to a solution containing an appropriate concentration of metal-free G6-OH. TEM images were obtained at 200 keV and a magnification of 250 000 in bright-field mode using a JEOL 2010F transmission electron microscope (TEM).

XAS experiments were performed at beamline X18B of the National Synchrotron Light Source at Brookhaven National Laboratory. In situ data were obtained under potential control using the previously described spectroelectrochemical cell. The XAS spectra were collected in fluorescence mode using an Ar-filled, five-grid Lytle detector, whereas reference spectra were obtained using Pt and Cu foils and collected in transmission mode. Prior to being fit, the X-ray absorbance edges for the in situ XAS data were aligned in energy with those for the reference foil spectra. XAS data were analyzed using the IFEFFIT6 sixPACK, ATOMS, and Horae software packages.[30−32] This software is available at no charge through the Consortium for Advanced Radiation Sources and is accessible online at http://cars9.uchicago.edu/ifeffit/Downloads.

■ RESULTS AND DISCUSSION

Basic Characterization of Pt DENs. The preparation and characterization of Pt DENs containing averages of 55, 147, and 225 atoms encapsulated within G6-OH PAMAM dendrimers followed procedures established in previous reports and briefly described in the Experimental Section.[23,33] Nanoparticles composed of an average of 55 and 147 atoms can form closed-shell cuboctahedra, and for convenience we assume that DENs are close approximations of this ideal structure.[34] The outermost shell of G6-OH(Pt_{55}) contains 42 Pt atoms, and the outermost shell of G6-OH(Pt_{147}) contains 92 Pt atoms. The next largest closed-shell cuboctahedron contains a total of 309 atoms; however, this is larger than the maximum number of Pt^{2+} ions that can coordinate within a single G6-OH dendrimer. This is because G6-OH dendrimers have, on average, 254 internal tertiary amines, and each tertiary amine can coordinate just one Pt^{2+} ion.[24] Note that 225 is a magic number for a truncated-octahedron, which has some structural characteristics in common to the cuboctahedron. Specifically, it has a face-centered cubic (fcc) crystal structure, presents (111) and (100) surface facets, and has 140 atoms located within its outermost shell (compared to 162 for a 309-atom cuboctahedron).[35]

UV−vis spectra of the G6-OH(Pt^{2+})$_n$ complexes were obtained before and after reduction with $NaBH_4$ (Supporting Information, Figure S6) and found to be in accord with previous reports.[23,33] TEM measurements and size-distribution histograms (Supporting Information, Figure S7) were also consistent with previous reports.[23,33] Specifically, the G6-OH(Pt_n) DENs, n = 55, 147, and 225, were found to have sizes of 1.5 ± 0.2, 1.9 ± 0.3, and 2.0 ± 0.3 nm, respectively.

Measurement of the Pt DEN Surface Area. Figure 1a shows CVs of a G6-OH(Pt_{55})-modified electrode before (black) UPD of a Cu monolayer, and then after UPD and stripping of Cu (red). Typical features associated with Pt electrochemistry are observed in both scans: Pt oxidation positive of 0.7 V, reduction of the oxide between 0.7 and 0.4 V, and hydrogen adsorption and desorption between 0.2 and 0 V. The near-superposition of the 2 CVs indicates that the Cu UPD process does not significantly affect the electrochemical surface area of the Pt DENs. Figure 1b and c show analogous CVs for GC electrodes modified with G6-OH(Pt_{147}) and G6-OH(Pt_{225}) DENs, respectively. As the size of the particles increases, the charge associated with Pt
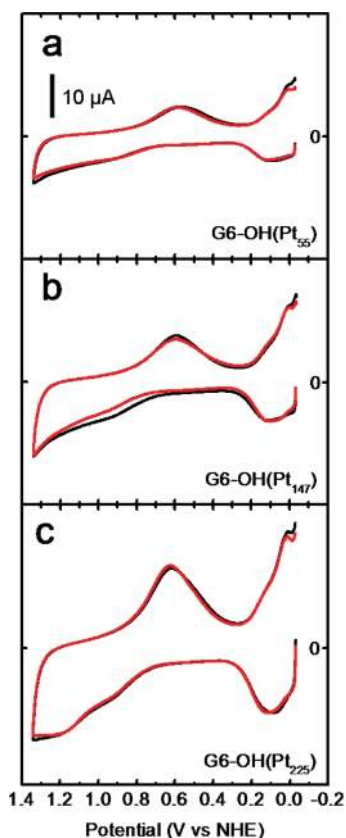
Figure 1. Cyclic voltammograms obtained using GC electrodes modified with the indicated G6-OH(Pt$_n$) DENs before (black) and after (red) Cu deposition and stripping. The aqueous 0.10 M H$_2$SO$_4$ electrolyte solution was deoxygenated with Ar. The scans started and ended at -0.03 V and were initially swept in the positive direction at a rate of 100 mV/s.

oxidation and reduction, as well as that for hydrogen adsorption and desorption, increases.

The total surface area of the three sizes of Pt DENs was determined by measuring the average charge, Q_H, due to hydrogen atom desorption before and after Cu UPD and stripping (between -0.03 and 0.32 V), and subtracting the capacitive charge (estimated using the current at 0.32 V). The value of Q_H was then converted to surface area using the widely accepted conversion factor of 210 μC/cm^2.[36] Note, however, that this latter value is only proven to be appropriate for bulk, polycrystalline Pt, and therefore the surface areas estimated for DENs must be considered with this caveat in mind.[37] The Pt surface areas determined before and after Cu UPD and stripping for a particular electrode are comparable (Table 1). These quantitative results are in accord with the voltammetry shown in Figure 1 and clearly demonstrate that Cu UPD and stripping do not affect the total Pt surface area. The results of a replicate study are presented separately (Supporting Information, Table S1). Although there are some differences in the measured surface areas, due to different numbers of immobilized DENs, the results from the replicate study are consistent with the data in Table 1.

The experimentally determined surface areas can be compared to a calculated estimate by making several assumptions:[33] (1) there is one nanoparticle per dendrimer; (2) the nanoparticles

are roughly spherical; (3) the projected area of the dendrimer on the electrode surface is 35 nm^2; (4) the dendrimers form a nearly close-packed monolayer on the GC electrode; and (5) the roughness factor of the GC electrode is 2.4.[33] The Pt surface areas calculated using these assumptions are 0.023, 0.043, and 0.065 cm^2 for immobilized G6-OH(Pt$_{55}$), G6-OH(Pt$_{147}$), and G6-OH(Pt$_{225}$), respectively. These values can be compared to the experimentally measured surface areas, determined from Q_H (Table 1) of 0.042, 0.081, and 0.10 cm^2, respectively. Given the approximations implicit to both the measured and calculated estimates, these values are in reasonable agreement.

Qualitative Analysis of the Voltammetry of Cu UPD on Pt DENs. Figure 2 displays the results of voltammetry obtained using the same Pt DEN-modified electrodes discussed in the previous section, but in Cu^{2+}-free and Cu^{2+}-containing 0.10 M H$_2$SO$_4$ solutions. These scans began at 0.64 V, proceeded positive to 0.84 V, reversed to 0.27 V, and then returned to 0.84 V. Others have used similar potential scan programs for Cu UPD onto bulk Pt.[28,29]

The black line in Figure 2a is a CV obtained using a G6-OH(Pt$_{55}$)-modified electrode in a Cu^{2+}-free, 0.10 M H$_2$SO$_4$ electrolyte solution. This CV was recorded immediately after the CV shown in black in Figure 1a, and it represents the background for the UPD experiment. This CV is featureless and displays only capacitive current. The CV corresponding to the red line in Figure 2a was obtained immediately following the background scan using the same electrode, but in the presence of 0.010 M Cu^{2+}. The Cu UPD current on G6-OH(Pt$_{55}$) manifests as a broad reduction wave having a peak potential of 0.40 V. Upon scan reversal, Cu is stripped from the Pt DENs: the first Cu oxidation wave has a peak potential of 0.38 V, and the second is at 0.52 V. The voltammetric profile for Cu UPD on G6-OH(Pt$_{147}$) (red trace, Figure 2b) is comparable to the results for G6-OH(Pt$_{55}$). However, the results for Cu UPD onto G6-OH-(Pt$_{225}$) are somewhat different. In this case, two distinct reduction waves and two oxidation waves are observed. A bulk, polycrystalline Pt electrode exhibits voltammetry very similar to G6-OH(Pt$_{225}$) (Supporting Information, Figure S8), and as discussed next the presence of two peaks may signal the evolution of faceting on the largest DEN.

Abruña and co-workers have observed surface-dependent voltammetric signatures for Cu UPD onto a Pt electrode having (111) and (100) facets in 0.10 M H$_2$SO$_4$ solution. They found two reduction waves and two oxidation waves, representing Cu UPD onto the two different Pt crystal facets.[4] The Cu UPD and stripping peaks on G6-OH(Pt$_{225}$) DENs also suggest a two-step deposition that we believe may correspond to Cu UPD on different surface features of the DENs. Presumably, these features are not well-enough developed on the smaller particles to exhibit this behavior.

The electrochemical properties of G6-OH(Pt$_{225}$) DENs with and without a Cu UPD shell were examined by voltammetry in 0.10 M H$_2$SO$_4$ (Figure 3). The experiment was carried out as follows. First, a G6-OH(Pt$_{225}$)-modified GC electrode was immersed in 0.10 M H$_2$SO$_4$ electrolyte solution and the potential was stepped from the OCP to 0.31 V and held there for 10 min before being swept from 0.31 V to -0.01 V and back to 0.31 V at a rate of 10 mV/s. The resulting CV, indicated by the red line in Figure 3, is dominated by the onset of the hydrogen-evolution reaction (HER) on the surface of G6-OH(Pt$_{225}$) DENs. Immediately after recording the CV shown in red, the electrode was moved to a solution containing 0.10 M H$_2$SO$_4$ + 0.010 M

Table 1. Variables Extracted from the Voltammetric Results Shown in Figures *1* and *2* for G6-OH(Pt$_n$) DENs and a Polycrystalline Pt Disk Electrode[a]

electrode		charge from H-des (μC)[b]	Pt SA (cm^2)[c]		charge from Cu UPD (μC)	θ_{Cu}	expected θ_{Cu} for complete shell[d]
G6-OH(Pt$_{55}$)	pre[e]	9	0.042	dep[g]	20		
	post[e]	9	0.042	strip[g]	24		
	Q_H[f]	9	0.042	Q_{Cu}[h]	22	1.2	2.2
G6-OH(Pt$_{147}$)	pre	16	0.076	dep	33		
	post	17	0.081	strip	33		
	Q_H	17	0.081	Q_{Cu}	33	1.0	1.8
G6-OH(Pt$_{225}$)	pre	22	0.10	dep	44		
	post	22	0.10	strip	44		
	Q_H	22	0.10	Q_{Cu}	44	1.0	1.7
polycrystalline Pt disk	pre	25	0.12	dep	51		
	post	25	0.12	strip	51		
	Q_H	25	0.12	Q_{Cu}	51	1.0	1.0

[a] The charge from H-des was measured in a Ar-purged 0.10 M H$_2$SO$_4$ electrolyte solution. The charge arising from Cu-UPD was measured in a Ar-purged 0.10 M H$_2$SO$_4$ + 0.010 M CuSO$_4$ electrolyte solution. [b] H-des is hydrogen desorption. [c] SA is surface area. [d] Expected θ_{Cu} calculated from the number of surface atoms in outer shells of model clusters. [e] Pre is the charge due to H-des measured before Cu UPD; post is the charge due to H-des measured after Cu UPD. [f] Q_H is the average of the pre and post H-des measurements. [g] Dep is the charge due to Cu deposition; strip is the charge due to Cu stripping. [h] Q_{Cu} is the average Cu UPD charge of the dep and strip measurements.
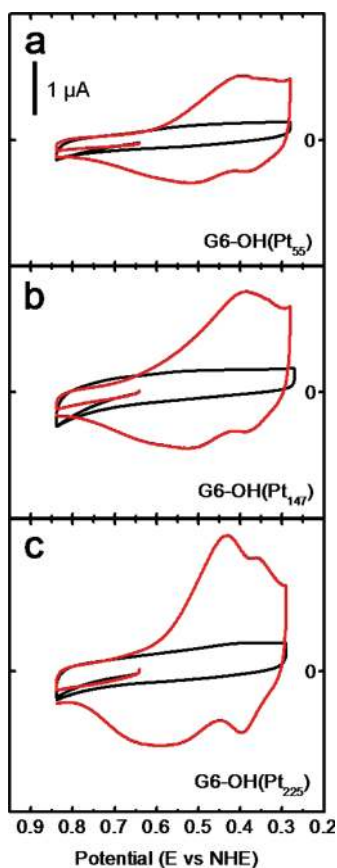

Figure 2. Cyclic voltammograms obtained using GC electrodes modified with the indicated G6-OH(Pt$_n$) DENs in aqueous electrolyte solutions containing 0.10 M H$_2$SO$_4$ only (black) and 0.10 M H$_2$SO$_4$ + 0.010 M CuSO$_4$ (red). The Cu UPD potential region is shown. The solutions were deoxygenated with Ar. The scans started at 0.64 V and were initially swept in the positive direction at a rate of 10 mV/s.
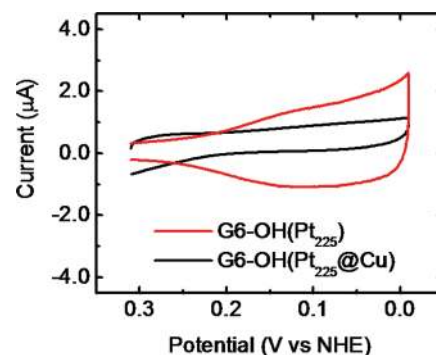

Figure 3. Cyclic voltammograms of G6-OH(Pt$_{225}$) DENs (red) and G6-OH(Pt$_{225}$@Cu) DENs (black) obtained in aqueous, Ar-purged 0.10 M H$_2$SO$_4$ electrolyte solutions. The scans began at 0.31 V and were initially swept in the negative direction at a rate of 10 mV/s.

CuSO$_4$, and a Cu shell was deposited onto G6-OH(Pt$_{225}$) DENs by stepping the electrode potential from 0.64 to 0.31 V and holding it there for 3 min. The electrode was then emersed from solution and immersed in a solution containing only 0.10 M H$_2$SO$_4$ under potential control (0.31 V), and then another CV was recorded. This latter CV, shown by the black line in Figure 3, reveals a featureless capacitance in the H adsorption/desorption region, indicating that the Cu shell blocks the HER. As an additional control measure, we also demonstrate that Cu UPD does not occur on GC electrodes modified only with empty (metal-free) G6-OH dendrimers (Supporting Information, Figure S9).

Quantitative Analysis of Cu UPD Coverage on Pt DENs. Because the electrodes used for Cu UPD measurements were the same as those used to measure the charge resulting from hydrogen desorption (Figure 1 and Table 1), the results of these two experiments can be directly compared. The charge resulting from Cu UPD and stripping (dep and strip,

respectively, in Table 1) was estimated from the voltammetric data in Figure 2 after subtracting the charge due to the background capacitance. The average charge resulting from Cu UPD and stripping, Q_{Cu}, is also listed in Table 1. The coverage of the Cu shell can be expressed as θ_{Cu} in eq 1.

$$\theta_{Cu} = \frac{N_{Cu}}{N_{Pt\text{-surf}}} = \frac{Q_{Cu}}{Q_H} \frac{ne_H}{ne_{Cu}} \qquad (1)$$

Here, θ_{Cu} is the ratio of Cu atoms in the shell (N_{Cu}) to the number of Pt atoms on the surface of the core ($N_{Pt\text{-surf}}$); Q_{Cu} is the average charge for Cu UPD and stripping (Table 1); Q_H is the average charge due to desorption of hydrogen atoms from the Pt surface before and after Cu UPD (Table 1); $ne_H = 1$ is the number of electrons required for oxidation of one adsorbed hydrogen atom, and $ne_{Cu} = 2$ is the number of electrons required for oxidation of one Cu atom.

To ensure that we are able to accurately measure θ_{Cu} on Pt DENs, it was also determined for a bulk, polycrystalline Pt electrode (Supporting Information, Figure S8). The result of this experiment is provided in Table 1, and it indicates $\theta_{Cu} = 1.0$ which is the expected result for Cu UPD onto bulk, polycrystalline Pt in H_2SO_4.[38]

The values of Q_{Cu} and Q_H for G6-OH(Pt_{55}) are 22 and 9 μC, respectively, yielding $\theta_{Cu} = 1.2$ (Table 1). The corresponding value of θ_{Cu} for both G6-OH(Pt_{147})- and G6-OH(Pt_{225})-modified electrodes is 1.0. (Table 1). This ratio is consistent with our results for Cu UPD on bulk, polycrystalline Pt (Supporting Information, Figure S8), previously reported measurements of Cu UPD onto Au DENs,[22] and literature reports of Cu UPD onto the low-index planes of Pt single crystals and polycrystalline Pt.[4,38,39]

The measured values of θ_{Cu} for Pt DENs merit some comment, because one might envision that θ_{Cu} could be larger. This is because outer shells of nanoparticles in the size range discussed in this project normally contain more atoms than inner shells. For example, a 55-atom cuboctahedral nanoparticle contains 42 atoms in the outermost shell, and the next full shell would contain 92 atoms. Therefore, G6-OH(Pt_{55}) could have a value of $\theta_{Cu} = 92/42 = 2.2$. The corresponding values of θ_{Cu} for G6-OH(Pt_{147}) and G6-OH(Pt_{225}) are calculated as $162/92 = 1.8$ and $234/140 = 1.7$, respectively.[34,40] We measure corresponding θ_{Cu} values of just 1.2, 1.0, and 1.0, suggesting that Cu UPD does not result in a fully closed outer shell covering the Pt DEN core. This could indicate that shell metals preferentially deposit onto the facets of DENs in a manner that is more characteristic of UPD on bulk single and polycrystalline Pt, perhaps leaving exposed some high-energy sites such as the edges and vertices of the nanoparticles. It is not clear why coverage on G6-OH(Pt_{55}) is higher than that for the other DENs, but more detailed structural studies are underway to address this issue. Finally, we carried out a second set of experiments intended to confirm those provided in Table 1. The detailed results are provided separately (Supporting Information, Table S1), but briefly the values of θ_{Cu} for G6-OH(Pt_n), $n = 55$, 147, and 225, were found to be 1.6, 1.1, and 1.0, respectively, in good agreement with those discussed here and presented in Table 1.

In Situ XAS Analysis of Cu UPD onto Pt DENs. We turned to in situ electrochemical XAS to confirm some of the preliminary structural conclusions derived from the previously discussed voltammetry experiments.[10,41,42] The experimental methodology for the XAS experiments was discussed earlier, but briefly, dialyzed G6-OH(Pt_{225}) DENs were immobilized on carbon
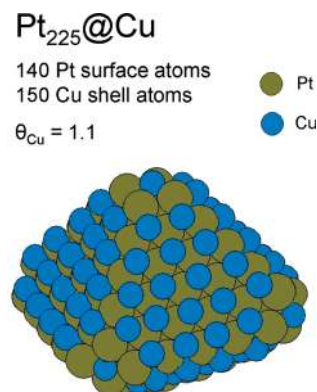
Scheme 2

$Pt_{225}@Cu$

140 Pt surface atoms
150 Cu shell atoms

$\theta_{Cu} = 1.1$

● Pt
● Cu

Table 2. Variables Extracted from in Situ XAS Spectra for G6-OH($Pt_{225}@Cu$)[a]

CN[b]	extracted CN[d]	calculated CN[e]	bond distance (Å)	Debye–Waller factor (Å^2)
n_{PP}	9.7 ± 1.4	9.5	2.75	0.006 + 0.0006
n_{PC}	1.3 ± 0.3	2.0	2.57	0.010 ± 0.003
n_{CC}	3.5 ± 1.6	4.2	2.62	0.014 ± 0.006
n_{CP}	3.4 ± 0.2	3.2	2.57	0.010 ± 0.003
n_{CE}[c]	1.0 ± 0.4	not calculated[f]	1.99	0.006 ± 0.005
n_{Pm}	11.0	11.5	N/A[g]	N/A
n_{Cm}	6.9	7.4	N/A	N/A

[a] All data were collected with the electrode poised at E_{UPD} in a 0.10 M H_2SO_4 solution. [b] CN is coordination number. [c] n_{CE} represents Cu with a low-Z nearest-neighbor. [d] Extracted CN is extracted from the fit to the data. [e] Calculated CN is estimated from the model $Pt_{225}@Cu$ structure with $\theta_{Cu} = 1.1$. [f] n_{CE} was not calculated because the concentration of low-Z nearest-neighbors (E) adsorbed to Cu has not been measured on $Pt_{225}@$ Cu structures. [g] Not applicable (N/A) to n_{Pm} and n_{Cm} because these CNs are sums of other CNs and are not variables included in the fit.

paper and the potential of this electrode was controlled during acquisition of XAS data. Because G6-OH(Pt_{225}) DENs are magic number clusters, the coordination numbers (CNs) obtained from the fits to the XAS data can be compared to those calculated for a model structure. The model is based on the quantitative electrochemical results discussed in the previous section. As shown in Scheme 2, it consists of a core containing 225 Pt atoms configured in a truncated-octahedron geometry. This structure has 140 Pt surface atoms distributed between eight (111) facets and six (100) facets. The Cu shell atoms are located exclusively on the facets, leaving the edges and vertices naked. Each Pt(111) facet accommodates 18 Cu atoms situated in 3-fold hollow sites, and each Pt(100) facet holds 1 Cu atom in a 4-fold hollow site. The value of θ_{Cu} for this model structure is $150/140 = 1.1$, which is close to θ_{Cu} measured from voltammetric data for G6-OH-(Pt_{225}) (Table 1). CNs can also be calculated for the model shown in Scheme 2, and these values are presented alongside the CNs extracted from the fits to the data (calculated and extracted, respectively, in Table 2).

The R-space distribution plots for G6-OH($Pt_{225}@Cu$) DENs, as well as the computed fits, are shown in Figure 4a and b for the Pt L3 and Cu K absorbance edges, respectively. These in situ XAS results were obtained with the DEN-modified electrode
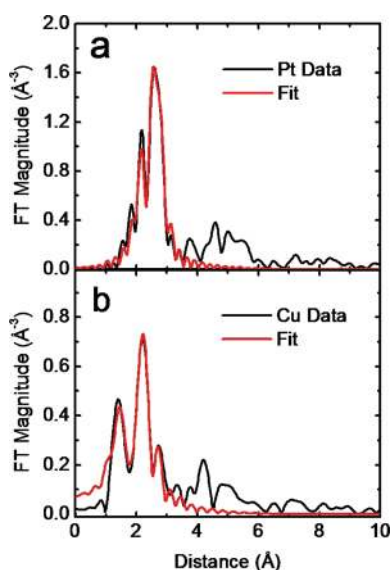
Figure 4. Radial distribution (R-space) spectra of the in situ XAS data for G6-OH(Pt_{225}@Cu) obtained under potential control in 0.10 M H_2SO_4 at E_{UPD}. The Pt data were fit using a k-space range of 3−15.5 and an R-window of 1.7−3.2. The Cu data were fit using a k-space range of 2−11 and an R-window of 1.2−3.224. Variables, such as the CN, bond distance, and Debye−Waller factors, were extracted from the fits to the data and are presented in Table 2.

held at E_{UPD} (0.26 V), which is the potential of maximum Cu UPD coverage. The corresponding k-space data are provided separately (Supporting Information, Figure S10).

The structure of the G6-OH(Pt_{225}@Cu) DENs is determined by fitting the XAS data, as described in the Experimental Section, and then comparing the extracted CNs to the values calculated for one or more models. The following CNs were extracted from the in situ spectra: Pt−Pt (n_{PP}), Pt−Cu (n_{PC}), Cu−Pt (n_{CP}), Cu−Cu (n_{CC}), Cu-E (n_{CE}), Pt-m (n_{Pm}), and Cu-m (n_{Cm}). Here, m is all metal (Pt plus Cu) and E is a low-Z nearest neighbor, most likely H_2O, HSO_4^-, or SO_4^{2-} on the Cu shell.[43] It was necessary to include the Cu-E scattering path to accurately fit the experimental results, but we did not calculate a CN corresponding to n_{CE}. One final point: the modeling approach assumes $n_{Pm} = n_{PP} + n_{PC}$ and $n_{Cm} = n_{CC} + n_{CP}$.[10,42]

Table 2 provides the extracted and calculated (for the model shown in Scheme 2) CNs, bond distances, and Debye−Waller factors for G6-OH(Pt_{225}@Cu). It is interesting to compare n_{PP} for G6-OH(Pt_{225}) at OCP and E_{bare}, before and after Cu UPD (Supporting Information, Figure S11), with n_{PP} for G6-OH-(Pt_{225}@Cu) at E_{UPD}. The experimental values for n_{PP} at OCP (CN = 7.0) and E_{bare} (CN = 6.9) underestimate the calculated CN for a 225-atom cluster (CN = 9.5),[44] but they are close to n_{PP} reported previously (CN = 6.3) for Pt DENs of similar size and under comparable conditions.[24,26]

At E_{UPD}, the calculated and extracted values of n_{PP} for G6-OH (Pt_{225}) are 9.5 and 9.7, respectively. The extracted CNs for n_{CC} and n_{CP} are also very close to the calculated values (Table 2). The extracted n_{PC} is lower than the calculated estimate by 0.7. The magnitude of the discrepancy between the calculated and extracted CNs is small and within the uncertainty of the fit. Such discrepancies are not unusual and may be due to disorder.[42] The value of n_{Pm} (11.0) is estimated as the sum of n_{PP} and n_{PC}. Likewise, n_{Cm} is 6.9. Both n_{Pm} and n_{Cm} are in good agreement with the corresponding CNs

that were calculated from the model: 11.5 and 7.4, respectively (Table 2).

From a modeling perspective, there are a few clear trends that distinguish core@shell nanoparticles from random arrangements such as alloys. For example, n_{PP} for G6-OH(Pt_n@Cu) and G6-OH(Pt_n) will be the same if the assumed structure of the former is core@shell. However, if the shell metal partitions into the core phase, n_{PP} will decrease.[10] Experimentally, we find that n_{PP} has the value calculated for a 225-atom truncated octahedron after addition of the Cu shell (Table 2), which is fully consistent with the proposed core@shell structure. We also know that the value of n_{Cm} will be less than n_{Pm} for a core@shell particle, because if Cu atoms are confined to the surface of the nanoparticle they will have fewer nearest neighbors than if they are randomly distributed throughout the particle.[10] Indeed, consistent with the core@shell structure, we find experimentally that n_{Pm} is quite significantly larger than n_{Cm} (Table 2).

The Debye−Waller factors given in Table 2 indicate 2-fold greater disorder in the Cu−Cu bonding than for Pt−Pt bonds. However, the Pt−Pt bond disorder for the core@shell DENs (Table 2) is similar to that observed for the monometallic Pt DENs at OCP (Supporting Information, Figure S11a). This is yet another indication that the core and shell phases of G6-OH(Pt_{225}@Cu) DENs are well-segregated. The coordinatively unsaturated atoms of the outer shells of nanoparticles occupy positions of higher energy and tend to exhibit greater disorder than the interior atoms of the nanoparticle, which have full coordination shells.[42]

The heterometallic (Pt−Cu) bond distance was determined to be 2.57 Å. We expect the Pt−Cu bond distance to lie between the Pt−Pt bond distance (2.77 Å) and Cu−Cu bond distance (2.55 Å).[41,42] Previous in situ XAS studies of Cu UPD on bulk Pt(111) reported a Pt−Cu bond distance of 2.64 Å.[45] The difference between the Pt−Cu bond distance reported here and the previously measured Pt−Cu bond distance (on a bulk Pt electrode) could be related to the strain-inducing effects of nanoparticle surface tension.[46,47] The Pt−Pt bond distance for G6-OH(Pt_{225}@Cu) extracted from the fit is 2.75 Å, which is close to that of Pt atoms in fcc Pt (2.77 Å). The Pt−Pt bond distance for bare G6-OH(Pt_{225}) at OCP and E_{bare} is also measured as 2.75 Å. This suggests a slight compression of the core Pt lattice. In contrast, the Cu−Cu bond distance is 2.62 Å, which is considerably larger than that expected for fcc Cu (2.55 Å). The lattice constant for fcc Pt is greater than that of Cu, and thus, it is likely that the Cu shell experiences some strain due to lattice mismatch with the underlying lattice of the Pt core.[46] Indeed, such strain has been observed in Cu overlayers in previous XAS studies of Cu UPD on bulk Pt(111).[43,45] Additionally, the compressive strain of the Pt lattice may be attributed to surface tension.[47] Nanoparticles exhibit surface tension resulting in lattice compression near the core, and calculations from theory predict a compression of the bond distance of about 1% for Pt nanoparticles having diameters around 2 nm.[47] The experimentally observed lattice compression for both G6-OH(Pt_{225}@Cu) (Table 2) and bare G6-OH(Pt_{225}) (Supporting Information Figure S11) amounts to 0.8%, which is consistent with these calculations.

The results of an independent replicate in situ XAS experiment returned CNs, bond distances, and Debye−Waller factors that are consistent with the results shown in Table 2. These results are provided in the Supporting Information, Table S2.

■ SUMMARY AND CONCLUSIONS

This study was motivated by recent findings that highly structured core@shell nanoparticles can be prepared using electrochemical methods.[3,13,14,16,18,19,21] We wanted to know if this same general approach could be applied to DENs, which are significantly smaller than previously reported materials. The successful outcome of these experiments provides a general method for synthesizing core@shell model nanoparticles that are sufficiently small and well-defined that their catalytic properties can be compared to first-principles calculations.[9]

We are now turning our attention to the aforementioned catalysis studies. In addition, experiments are underway to determine if this same UPD approach can be used to prepare core@-shell DENs having different compositions. Finally, we are particularly excited by the prospect of using electrosynthesis to selectively activate or poison particular facets of DENs containing as few as 55 atoms. Findings from these continuing experiments will be reported in due course.

■ ASSOCIATED CONTENT

ⓢ Supporting Information. UV–vis spectra, TEM images, cyclic voltammograms, XAS data, and diagrams of the electrochemical cells. This material is available free of charge via the Internet at http://pubs.acs.org.

■ AUTHOR INFORMATION

Corresponding Author

*E-mail: crooks@cm.utexas.edu. Telephone: 512-475-8674.

■ ACKNOWLEDGMENT

■ REFERENCES

(1) Scott, R. W. J.; Wilson, O. M.; Crooks, R. M. *J. Phys. Chem. B* **2005**, *109*, 692–704.

(2) Rodríguez-López, M.; Solla-Gullón, J.; Herrero, E.; Tuñón, P.; Feliu, J. M.; Aldaz, A.; Carrasquillo, A. *J. Am. Chem. Soc.* **2010**, *132*, 2233–2242.

(3) Sasaki, K.; Mo, Y.; Wang, J. X.; Balasubramanian, M.; Uribe, F.; McBreen, J.; Adzic, R. R. *Electrochim. Acta* **2003**, *48*, 3841–3849.

(4) Gómez, R.; Feliu, J. M.; Abruña, H. D. *Langmuir* **1994**, *10*, 4315–4323.

(5) Kowal, A.; Li, M.; Shao, M.; Sasaki, K.; Vukmirovic, M. B.; Zhang, J.; Marinkovic, N. S.; Liu, P.; Frenkel, A. I.; Adzic, R. R. *Nat. Mater.* **2009**, *8*, 325–330.

(6) Andersson, K. J.; Calle-Vallejo, F.; Rossmeisl, J.; Chorkendorff, I. *J. Am. Chem. Soc.* **2009**, *131*, 2404–2407.

(7) Greeley, J.; Mavrikakis, M. *J. Phys. Chem. B* **2005**, *109* 3460–3471.

(8) Ferrin, P. A.; Kandoi, S.; Zhang, J.; Adzic, R. R.; Mavrikakis, M. *J. Phys. Chem. C* **2009**, *113*, 1411–1417.

(9) Tang, W.; Henkelman, G. *J. Chem. Phys.* **2009**, *130*, 194504.

(10) Weir, M. G.; Knecht, M. R.; Frenkel, A. I.; Crooks, R. M. *Langmuir* **2010**, *26*, 1137–1146.

(11) Wilson, O. M.; Scott, R. W. J.; Garcia-Martinez, J. C.; Crooks, R. M. *J. Am. Chem. Soc.* **2004**, *127*, 1015–1024.

(12) Adzic, R. R.; Zhang, J.; Sasaki, K.; Vukmirovic, M. B.; Shao, M.; Wang, J. X.; Nilekar, A. U.; Mavrikakis, M.; Valerio, J. A.; Uribe, F. *Top. Catal.* **2007**, *46*, 249–262.

(13) Yu, Y.; Hu, Y.; Liu, X.; Deng, W.; Wang, X. *Electrochim. Acta* **2009**, *54*, 3092–3097.

(14) Jin, Y.; Shen, Y.; Dong, S. *J. Phys. Chem. B* **2004**, *108*, 8142–8147.

(15) Lima, F. H. B.; Zhang, J.; Shao, M. H.; Sasaki, K.; Vukmirovic, M. B.; Ticianelli, E. A.; Adzic, R. R. *J. Phys. Chem. C* **2007**, *111*, 404–410.

(16) Shao, M. H.; Huang, P. L.; Zhang, J.; Sasaki, K.; Vukmirovic, M. B.; Adzic, R. R. *Langmuir* **2006**, *22*, 10409–10415.

(17) Vukmirovic, M. B.; Zhang, J.; Sasaki, K.; Li, M.; More, K.; Adzic, R. R. *ECS Trans.* **2008**, *13*, 3–12.

(18) Wang, J. X.; Inada, H.; Wu, L.; Zhu, Y.; Choi, Y.; Liu, P.; Zhou, W.-P.; Adzic, R. R. *J. Am. Chem. Soc.* **2009**, *131*, 17298–17302.

(19) Lee, J.; Hwang, S.; Hongji, L.; Kwak, J. *J. Phys. Chem. B* **2004**, *108*, 5372–5379.

(20) Liu, P.; Ge, X.; Wang, R.; Ma, H.; Ding, Y. *Langmuir* **2009**, *25*, 561–567.

(21) Sasaki, K.; Wang, J. X.; Naohara, H.; Marinkovic, N.; More, K.; Inada, H.; Adzic, R. R. *Electrochim. Acta* **2009**, *55*, 2645–2652.

(22) Yancey, D. F.; Carino, E. V.; Crooks, R. M. *J. Am. Chem. Soc.* **2010**, *132*, 10988–10989.

(23) Ye, H.; Crooks, R. M. *J. Am. Chem. Soc.* **2005**, *127*, 4930–4934.

(24) Knecht, M. R.; Weir, M. G.; Myers, V. S.; Pyrz, W. D.; Ye, H.; Petkov, V.; Buttrey, D. J.; Frenkel, A. I.; Crooks, R. M. *Chem. Mater.* **2008**, *20*, 5218–5228.

(25) Kiema, G. K.; Aktay, M.; McDermott, M. T. *J. Electroanal. Chem.* **2003**, *540*, 7–15.

(26) Weir, M. G.; Myers, V. S.; Frenkel, A. I.; Crooks, R. M. *ChemPhysChem* **2010**, *11*, 2942–2950.

(27) Solla-Gullón, J.; Lafuente, E.; Aldaz, A.; Martínez, M. T.; Feliu, J. M. *Electrochim. Acta* **2007**, *52*, 5582–5590.

(28) Green, C. L.; Kucernak, A. *J. Phys. Chem. B* **2002**, *106* 1036–1047.

(29) Danilov, A. I.; Molodkina, E. B.; Polukarov, Y. M.; Climent, V.; Feliu, J. M. *Russ. J. Electrochem.* **1998**, *34*, 1257–1261.

(30) Newville, M. *J. Synchrotron Radiat.* **2001**, *8*, 322–324.

(31) Ravel, B.; Newville, M. *J. Synchrotron Radiat.* **2005**, *12*, 537–541.

(32) Ravel, B. *J. Synchrotron Radiat.* **2001**, *8*, 314–316.

(33) Ye, H.; Crooks, J. A.; Crooks, R. M. *Langmuir* **2007**, *23* 11901–11906.

(34) Martin, T. P.; Bergmann, T.; Göhlick, H.; Lange, T. *J. Phys. Chem.* **1991**, *95*, 6421–6429.

(35) Wolfe, R. L.; Murray, R. W. *Anal. Chem.* **2006**, *78*, 1167–1173.

(36) Schmidt, T. J.; Gasteiger, H. A.; Stäb, G. D.; Urban, P. M.; Kolb, D. M.; Behm, R. J. *J. Electrochem. Soc.* **1998**, *145*, 2354–2358.

(37) Pozio, A.; De Francesco, M.; Cemmi, A.; Cardellini, F.; Giorgi, L. *J. Power Sources* **2002**, *105*, 13–19.

(38) Herrero, E.; Buller, L. J.; Abruña, H. D. *Chem. Rev.* **2001**, *101*, 1897–1930.

(39) Danilov, A. I.; Molodkina, E. B.; Polukarov, Y. M.; Climent, V.; Feliu, J. M. *Electrochim. Acta* **2001**, *46*, 3137–3145.

(40) Hostetler, M. J.; Wingate, J. E.; Zhong, C.-J.; Harris, J. E.; Vachet, R. W.; Clark, M. R.; Londono, J. D.; Green, S. J.; Stokes, J. J.; Wignall, G. D.; Glish, G. L.; Porter, M. D.; Evans, N. D.; Murray, R. W. *Langmuir* **1998**, *14*, 17–30.

(41) Myers, S. V.; Frenkel, A. I.; Crooks, R. M. *Chem. Mater.* **2009**, *21*, 4824–4829.

(42) Knecht, M. R.; Weir, M. G.; Frenkel, A. I.; Crooks, R. M. *Chem. Mater.* **2008**, *20*, 1019–1028.

(43) Yee, H. S.; Abruña, H. D. *J. Phys. Chem.* **1994**, *98*, 6552–6558.

(44) Glasner, D.; Frenkel, A. I. *XAFS 13, Proc. Int. Conf. X-ray Absorpt. Fine Struct.* **2007**, *882*, 746–748.

(45) Yee, H. S.; Abruña, H. D. *J. Phys. Chem.* **1993**, *97*, 6278–6288.

(46) Mavrikakis, M.; Hammer, B.; Nørskov, J. K. *Phys. Rev. Lett.* **1998**, *81*, 2819–2822.

(47) Jiang, Q.; Liang, L. H.; Zhao, D. H. *J. Phys. Chem. B* **2001**, *105*, 6275–6277.

■ NOTE ADDED AFTER ASAP PUBLICATION

This article was published ASAP on March 8, 2011. The caption to Figure 1 has been modified. The correct version was published on March 14, 2011.